Environmental Science & Technology

Article

pubs.acs.org/est

Demonstration of an Ethane Spectrometer for Methane Source Identification

Tara I. Yacovitch,[†] Scott C. Herndon,*[,†] Joseph R. Roscioli,[†] Cody Floerchinger,[†] Ryan M. McGovern,[†] Michael Agnese,[†] Gabrielle Pétron,[‡,#] Jonathan Kofler,[‡,#] Colm Sweeney,[‡,#] Anna Karion,[‡,#] Stephen A. Conley,[§] Eric A. Kort,[∥] Lars Nähle,[⊥] Marc Fischer,[⊥] Lars Hildebrandt,[⊥] Johannes Koeth,[⊥] J. Barry McManus,[†] David D. Nelson,[†] Mark S. Zahniser,[†] and Charles E. Kolb[†]

[†]Aerodyne Research Inc., Billerica, Massachusetts 01821, United States

[‡]Cooperative Institute for Research in Environmental Sciences, University of Colorado, Boulder, Colorado 80309, United States

[#]NOAA Earth System Research Laboratory, Boulder, Colorado 80305, United States

[§]University of California, Davis, California 95616, United States

[∥]Department of Atmospheric, Oceanic and Space Sciences, University of Michigan, Ann Arbor, Michigan 48109, United States

[⊥]Nanoplus Nanosystems and Technologies GmbH, Gerbrunn 97218, Germany

Supporting Information

ABSTRACT: Methane is an important greenhouse gas and tropospheric ozone precursor. Simultaneous observation of ethane with methane can help identify specific methane source types. Aerodyne Ethane-Mini spectrometers, employing recently available mid-infrared distributed feedback tunable diode lasers (DFB-TDL), provide 1 s ethane measurements with sub-ppb precision. In this work, an Ethane-Mini spectrometer has been integrated into two mobile sampling platforms, a ground vehicle and a small airplane, and used to measure ethane/methane enhancement ratios downwind of methane sources. Methane emissions with precisely known sources are shown to have ethane/methane enhancement ratios that differ greatly depending on the source type. Large differences between biogenic and thermogenic sources are observed. Variation within thermogenic sources are detected and tabulated. Methane emitters are classified by their expected ethane content. Categories include the following: biogenic (<0.2%), dry gas (1−6%), wet gas (>6%), pipeline grade natural gas (<15%), and processed natural gas liquids (>30%). Regional scale observations in the Dallas/Fort Worth area of Texas show two distinct ethane/methane enhancement ratios bridged by a transitional region. These results demonstrate the usefulness of continuous and fast ethane measurements in experimental studies of methane emissions, particularly in the oil and natural gas sector.

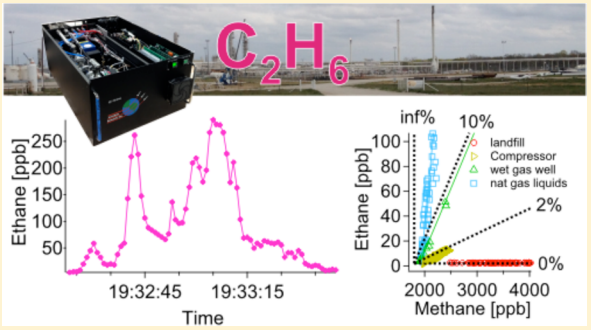

INTRODUCTION

Methane, an important greenhouse gas, is the primary component of natural gas (NG). With the increase in US natural gas exploration and production,[1] a number of studies aimed at quantifying methane emissions and improving global and national methane inventories have been published or are in progress.[2−6] A synthesis of 20 years of published research on US methane emissions points to a recurring underestimation of official inventories,[7] including thermogenic emissions from fossil fuel extraction and refining and biogenic emissions from ruminants and associated manure.[8] Practically, methane emissions from thermogenic oil and natural gas sources are often colocated with other biogenic sources of methane such as livestock, landfills, wetlands, or stagnant water. Atmospheric studies of methane sources need to be able to distinguish between different methane source types to quantify their respective contributions to ambient levels and overall regional emissions. One method of distinguishing biogenic and thermogenic methane sources is to use the presence of coemitted hydrocarbons such as ethane and propane to indicate an oil and gas source.[8] Furthermore, natural gas can contain varying amounts of condensable species. Industry convention classifies natural gas wells that are not associated with crude oil extraction into "wet" and "dry" gas wells, producing greater and lesser quantities of NG liquids, respectively. NG liquids include ethane, propane, normal and isobutanes, and other heavier hydrocarbons.[9]

The presence of other alkanes with methane from oil and natural gas reservoirs has been leveraged by industry in the

Received: March 26, 2014
Revised: June 13, 2014
Accepted: June 19, 2014
Published: June 19, 2014

exploration stage for its predictive powers on the type of resources contained in the geologic formation.[10] On the emissions monitoring side, gas chromatography (GC) of ethane and other non-methane hydrocarbons (NMHCs) from ambient air flasks and direct NG samples has provided evidence of the oil and gas industry's impact on methane emissions at both the global[11,12] and regional scales.[3,5,13−15] Such discrete flask sampling is limited in both the number of samples that it is possible to acquire and process, and the often significant delay between sample acquisition and analysis. Discrete sampling also cannot capture the full plume structure of continuous methane observations, hindering attribution studies from mobile vehicle and airborne platforms. Here we present a newly developed ethane spectrometer capable of reporting a continuous 1 s ethane mixing ratio with sub-ppb precision. We demonstrate its use in a ground vehicle and small aircraft. Emissions from precisely known methane sources are used to show that biogenic and thermogenic sources can be immediately distinguished and that thermogenic sources can be further characterized based on ethane content.

INSTRUMENT AND MEASUREMENT PERFORMANCE

Description. The analytical method used to quantify ethane in sampled ambient air is based on tunable infrared laser direct absorption spectroscopy (TILDAS).[16−18] This work discusses two deployment contexts: as part of the Aerodyne Mobile Laboratory[19,20] (AML) and aloft, aboard the Mooney TLS Bravo operated by Scientific Aviation, Inc.

The prototype ethane spectrometer is based on an adapted "mini QCL chassis" manufactured by Aerodyne Research, Inc.[21] and draws upon previously demonstrated techniques for continuous ethane measurement.[22,23] This apparatus consists of a computer controlled data acquisition system that synchronously controls a 3.3 μm distributed feedback tunable diode laser (DFB-TDL) from Nanoplus Nanosystems and Technologies GmbH,[24] coupled to an astigmatic multipass absorption cell.[25] The multipass absorption cell used for the measurements described here was aligned to produce an absorption path length of 76.0 m. Spectra are obtained by sweeping the laser current for 800 steps, each with a duration of 632 ns (1.5 MHz per channel). The subsequent 60 channels were collected with sub-threshold current to the laser to dynamically quantify the zero signal of the infrared detector.

The acquisition process is repeated at a repetition rate of 1.8 kHz. At a user selectable interval (0.1 and 1 s are typical), the resulting averaged spectrum is processed using a nonlinear least-squares fitting algorithm to determine mixing ratios. The analysis uses a measured tuning rate acquired with an etalon spectrum to convert between measured channel number and relative wavenumber. The absolute wavenumber to channel offset in this work is determined as a fit parameter either in the signal spectrum or during reference spectra acquisition (described later).

Ethane mixing ratios are determined from a multicomponent fit of the absorption spectrum. This fit includes weak methane absorption lines to account for the feature that overlaps with the ethane lines. Further details of the fit are described in the SI. The ethane spectral feature being monitored consists of many overlapping spectral lines (Figure 1, Panel A). Each line was modeled with a Voigt absorption profile[26] calculated using the measured pressure and temperature of the gas in the multipass cell. The spectroscopic constants were taken from

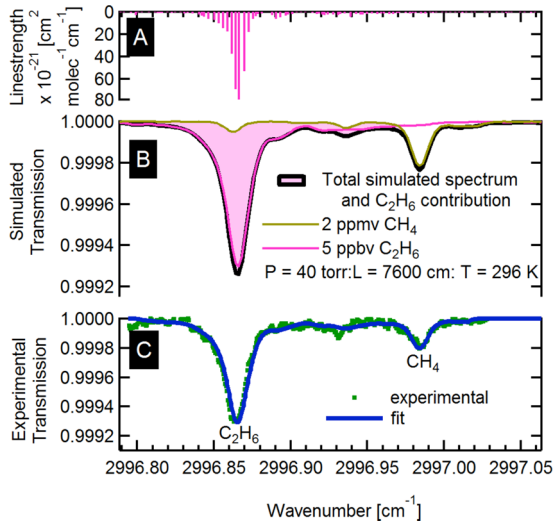

Figure 1. Simulated and experimental ethane spectra. The ethane line spectrum is shown in Panel A and the resulting simulation in Panel B. The total spectrum (black) includes contributions from ambient levels of water (1.3%), CO_2 (350 ppm), N_2O (320 ppb), and O_3 (30 ppb), though only the CH_4 (2 ppm) and C_2H_6 (5 ppb) are apparent. Panel C shows the average experimental signal intensity (green points) from 1538 spectra (~1 s interval) acquired at 37 Torr and 297 K. The solid blue line is the result of the solution to the Beer−Lambert absorption model combined with a low order polynomial background.

Harrison et al.[27] since the current HITRAN database[28] does not satisfactorily reproduce[27] the ethane spectrum in the 3 μm region. An example experimental spectrum is depicted in Figure 1, Panel C. The spectrum was acquired with a cell pressure of 37 Torr at 297 K and with a flow rate of 8.1 standard liters per minute (slpm). Although the absorption feature at 2996.87 cm^{-1} looks like a single line, it is the accumulated absorption of several pressure-broadened rotation-vibration transitions within a Q-branch manifold.

In operation, the laser is locked to a specific wavelength, using either the sample spectrum (if the absorption depth due to ambient ethane is sufficiently strong) or using a reference cell. In the latter case, a flip-in reference cell containing ethane is mechanically triggered into the light path every 2 min for two seconds in order to quantify the precise relationship between the acquisition channel and ethane line-center when sampling in regions where the ethane mixing ratio is lower than ~2 ppb. In either case, the frequency lock is achieved using a semiproportional-integral-derivative feedback algorithm running as part of the data acquisition system.

When deployed aboard the AML, the typical mass flow rate through the instrument was 7−9 slpm. The calculated volumetric sample response time of the multipass absorption cell is <300 ms. On the aircraft, with a smaller pump, the mass flow rate was ~3 slpm corresponding to a response time of ~600 ms. Empirical tests of the response times confirm that the instrument response is much less than the apparent duration of plume encounters described in the analysis below (5−300 s). These tests consist of a triggered valve "overblow" with hydrocarbon-free air or calibration gas delivered as close to the inlet tip as possible and upstream of all instruments.

In each of the mobile laboratory and airborne deployments, the instrument triggers a valve that overblows the inlet every 15 min with compressed air that is virtually ethane free. These

events typically last for 15 to 30 s. The recorded "background" spectrum was used to normalize the subsequent sample spectra.

Methane mixing ratios in the Mobile Laboratory are quantified using the Aerodyne mid-IR quantum cascade laser instrument[29,30] operated in series with the ethane instrument. Methane mixing ratios in the aircraft-based measurements are determined using a Picarro model 2401-m cavity ring-down spectrometer (CRDS).[31] Additional details of the mobile sampling platform integrations are available in the SI.

Performance and Calibration. The 1 s noise in the ethane mixing ratio for these studies ranges from 19 to 210 ppt, depending on the particular circumstances of the measurement. Typical ambient ethane mixing ratios measured in these field studies are in excess of 4 ppb, leading to signal-to-noise ratios of 19 and higher. The conclusions of this study thus do not depend significantly upon the noise performance of the instrument. In Figure 2, Allan variance plots[32] (variance, σ^2, vs averaging time) are shown for the instrument in three different circumstances. The best noise performance of σ = 19 ppt in 1 s was achieved with the instrument mounted for flight, but while stationary and overblowing the inlet with ethane-free air (blue trace). In flight, the noise was 4 times higher (green trace). When the instrument was mounted in the AML, and in motion, the noise can be significantly higher, e.g. 210 ppt, as seen in the red trace in Figure 2. The flight and AML data segments were chosen to have stable ambient ethane levels (green and red traces in Figure 2). Increased noise while in motion may have multiple root causes, all of which ultimately act on the spectrum and cause changes to properties such as optical baseline shape or interference fringes. The degree of alignment, presence of vibrational isolation, intensity of accelerations and temperature stability of the instrument may all affect the spectrum. We attribute the reduced noise in the aircraft versus the AML to a combination of these factors (see the SI).

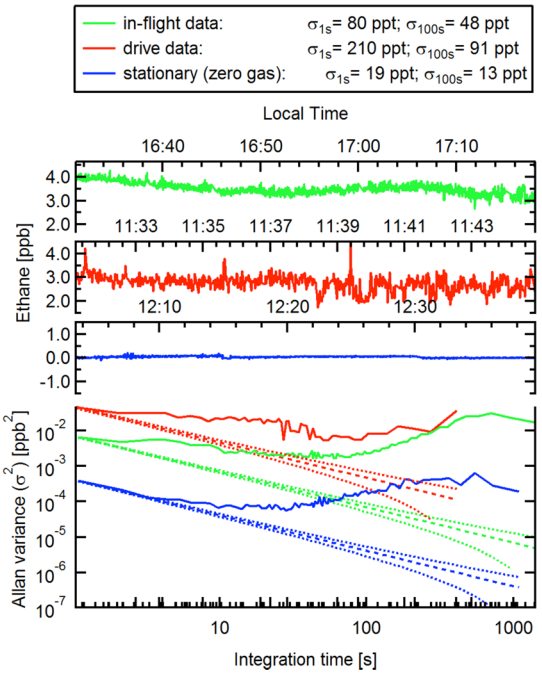

Figure 2. Noise performance in motion while sampling ambient air in the Mooney TLS Bravo aircraft (green) and the AML (red). Stationary noise performance while sampling ethane-free air is also shown (blue). Ethane time traces (top three traces) are shown above the experimental variance (solid lines). The Allan variances of a sample with purely random variations are shown for comparison with 95% confidence limits (dotted lines).

The reported ethane/methane ratios reported within have not been externally calibrated, though instrument performance is routinely monitored against standards. The Ethane-Mini instrument accuracy has been tested against three standards containing ethane in mixing ratios of 1060, 1000.0 (0.5), and 17.57 ppb, respectively (error, when available, is reported as a standard deviation of the mean). The low-mixing ratio standard is a tank of compressed air that was sampled and had its value assigned on the Irvine scale.[33,34] All calibration tanks also contain near-ambient levels of methane, N_2O and CO_2. Direct overblow of the instrument inlet with these tanks resulted in the recovery of the tank mixing ratios with factors of 0.924, 0.987, and 0.979 respectively. Quantitative dilution calibrations were also performed for the 1000 ppb tank (see the SI), yielding a factor of 0.937. These calibration factors suggest that the instrument systematically underestimates the ethane mixing ratio by ~6%. In the determination of ethane/methane enhancement ratios, the methane calibration factor is also important. A methane standard of 500 ppm was quantitatively diluted, as above, and yields a calibration factor of 0.973. Ethane/methane enhancement ratios are thus expected to be systematically low by ~4% (by taking the ratio of the calibration factors). An uncertainty of ±4% is estimated for the ethane absorption cross sections for the lines shown in Figure 1.[27] Until additional calibration protocols are developed and these calibration factors rigorously reproduced under a wide range of conditions, we report the spectroscopically determined mixing ratio without external calibration adjustment and recommend instead that an additional 6% systematic error be considered in addition to the reported statistical errors.

RESULTS AND DISCUSSION

The ethane content of a methane plume reveals information about its source. In the following sections, ethane content is expressed as a percentage of emitted methane (ppb/ppb · 100%). This work focuses on the analysis of plumes encountered by the two measurement platforms described above. The plume encounter is defined as an enhancement of methane above background (before and after the plume). A scatter plot of the ethane vs methane measurements is used here to determine the ethane/methane enhancement ratio of a source. The slope of the scatter plot determines the enhancement ratio of ethane to methane in the source. No background value is assumed in this analysis. Correlation of the time-traces corrects for the minor shift in data acquisition time due to different sampling points along the inlet (<~2 s). A good correlation coefficient (as identified by a high R^2 of the linear fit, >0.65 in these results) is an indication that both ethane and methane have undergone equivalent dilution during atmospheric dispersion and thus originate from the same source.

An equivalent analysis of the ethane content of plumes can be done by drawing on techniques used for isotope analyses. If ethane is considered as an "isotope" of methane, then an ethane del (δC_2) can be devised such that $\delta C_2 = (C_2/C_1)\cdot 100\%$, where C_2 and C_1 are the mixing ratios of ethane and methane in the sample, respectively (see the SI). The intercept of the Keeling plot[35] of δC_2 vs $1/C_1$ gives the source ethane/methane enhancement ratio.

Measurement of Known Sources. Three measured methane plumes from precisely known emitters are shown in Figure 3 below. Data were collected on the Aerodyne Mobile Laboratory[19] by transecting emission plumes downwind. Wind measurements were acquired on-board to help pinpoint the source location. The equipment or facility description and NG characteristics for the two oil and gas emitters were additionally confirmed by on-site operators.

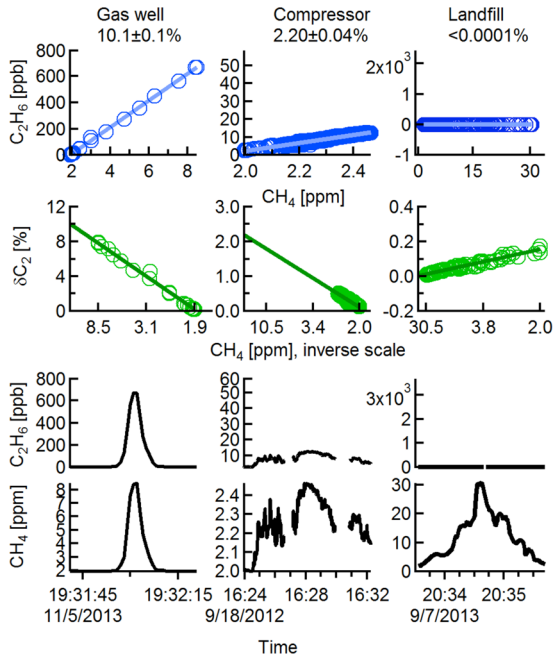

Figure 3. Ethane content of methane emissions for three known sources. The slopes of ethane (C_2H_6) vs methane (CH_4) (blue markers and fit lines) are shown in the top panel. An equivalent analysis using a Keeling-like plot of ethane del (δC_2) vs $1/CH_4$ is also shown. The $1/CH_4$ axis is linear but is labeled with the methane concentration for ease of reading. The corresponding ethane and methane time traces are shown below. The range of each ethane axis is set to 12% of the range of the associated methane axis.

The first source is a NG well pad in the western US, producing gas that is rich in NMHCs (aka "wet gas"). The second source is a compressor station in the northeastern US, operating on NG that is ready for distribution. The last is a municipal landfill near Dallas/Fort Worth. Though the methane enhancements over background downwind of these point sources vary greatly in magnitude and in duration, the ethane axis ranges in Figure 3 are fixed to 12% of the associated methane range in order to show the great variability in ethane content between sources. The ethane contents for these three methane plumes are 10.1 ± 0.1% for the wet gas well; 2.20 ± 0.04% for the compressor station; and smaller than 0.0001% for the landfill, as determined from the slopes of the correlation plots. Comparable values are measured with intercepts of the Keeling-like plots (see the SI). The error values reported above are derived from the standard deviation of the slope and expressed at the 95% confidence level. This does not reflect the overall systematic uncertainty in the measurements of ∼6% (see Performance and Calibration section above). The ethane trace for the landfill plume shows poor correlation between the intense methane plume and the ethane baseline (R^2 of the fit is 0.24), and so we report only an upper confidence limit to the enhancement ratio.

The ethane content of these three different methane source types differs by orders of magnitude. The landfill is a prime example of a biogenic methane source, where emissions come from methanogenic bacteria. It contains virtually no ethane. Other such sources include livestock rumination, manure and biomass composting, rice paddies, wastewater treatment facilities, and wetlands. The compressor station, with 2.20% ethane, is an example of distribution-ready NG. This measured value agrees (within ∼10%) with operator data from well-pads feeding this compressor station. The wells were producing dry gas (low in NMHCs) and the gas did not require any significant processing (such as ethane removal) prior to being sent to the

Table 1. Observed Ethane/Methane Enhancement Ratios and Emission Category

example	measured ethane/methane enhancement ratio[a,d]	emission category	category range of ethane/methane enhancement ratio
municipal landfill, Figure 3	<0.0001%		
wastewater treatment facility, Dallas Fort-Worth	<0.01%	biogenic	<0.2%[42]
stagnant water, Houston area	<0.05%		
liquefied natural gas (LNG) tank venting	0.029%	LNG	<6%[36]
city of Boston gas leaks, Boston University rooftop	1.8−2.3%		
compressor station, Figure 3	2.20%	pipeline grade NG	<15%[37,38]
14 Compressor stations[b,c4]	1.0−3.5%[c]		
well field, Wellsboro PA region[2]	2.38%	dry gas[b]	1−6%[e]
gas well, western US, Figure 3	10.1%	wet gas[b]	>6%[e]
NG processing plant, western US	44.7%	processed NG liquids	>30%[e]
chemical plant feedstock, Houston area	∞%	hazardous liquids pipeline	∞%

[a]See the SI for data supporting these measurements. [b]Wet and dry-gas examples are for well sites not predominantly associated with oil production. [c]Operator gas analysis data for the 14 compressor stations states a range of ethane contents 0.9−4.5% (see the SI). [d]Results limited to the region and time frame sampled. [e]Range estimates.

compressor. Finally, the NG well plume shows the highest ethane content of all three sample plumes, consistent with the release/leak of a "wet" gas rich in NMHCs. Gas with this composition may undergo midstream processing to separate and collect NMHCs before injection into the transmission system.

Figure 3 shows that even small enhancement ratios of ethane can clearly distinguish oil and gas sources from a biogenic methane plume, devoid of NMHCs. With combined 1 s ethane and methane measurements, this determination can be done immediately as a plume of methane and ethane is encountered in the field and can be used to direct the focus of methane emissions studies. The differences in the ethane/methane enhancement ratios between the compressor station and gas well demonstrate a further potential for real-time ethane measurements: refinement of the source type of an unknown oil and gas sector emitter.

Though the ethane/methane enhancement ratio alone cannot identify an unknown plume's source, it can narrow down the possible source types. To this end, select ethane/methane enhancement ratios and their source types are presented in Table 1 below. All examples shown come from known and verified sources, with time traces, correlation plots, and additional relevant information present in the SI. The measured ethane/methane enhancement ratios are roughly grouped by category.

Biogenic sources like the landfill, wastewater treatment plant, and stagnant water are expectedly absent of ethane within the detection limit. Two categories of emissions have ethane/methane enhancement ratios that are strongly influenced by regulations and industry agreements on transport and heating capacity: liquefied natural gas (LNG) and pipeline grade NG.[36−39] The dry gas and wet gas categories refer to unprocessed NG from wells not predominantly associated with oil production, containing lower or higher NMHC content depending on the characteristics of the geologic formation.[10] At ethane/methane enhancement ratios in excess of ∼30%, we mainly find emissions sources having to do with the processing of NG liquids, including so-called NG plant liquids and plant condensates.[9] As these liquids undergo processing, their composition can range from mixed liquid hydrocarbons to purified chemical products, which may be transported in dedicated pipelines, such as pure ethane for the synthesis of ethylene.[40] Emissions from the venting of oil storage tanks (flashing) are separated from these NG liquids categories due to the expected differences in vapor composition.[41]

Measurement of Regional Enhancement Ratio Downwind of Dallas/Fort Worth Region. In Figure 4, an entire region made up of a complex mix of emitters is sampled. The Dallas/Fort Worth Region in Texas is home to the Barnett shale formation, where horizontal drilling and hydraulic fracturing have allowed for the extraction of NG and oil. In this major metropolitan area, there are also other sources such as landfills contributing to regional methane emissions. The map in Panel B of Figure 4 shows the boundaries of the Barnett shale (dotted line) bisecting Dallas and Fort Worth north−south.

The ethane spectrometer was installed into the cargo area of a small Mooney airplane (see the SI). An approximately perpendicular east−west transect of the Barnett plume was chosen for this demonstration. The plane's trajectory, which was at constant altitude within the boundary layer, is shown as a thick black trace in Figure 4. The measured south-to-north

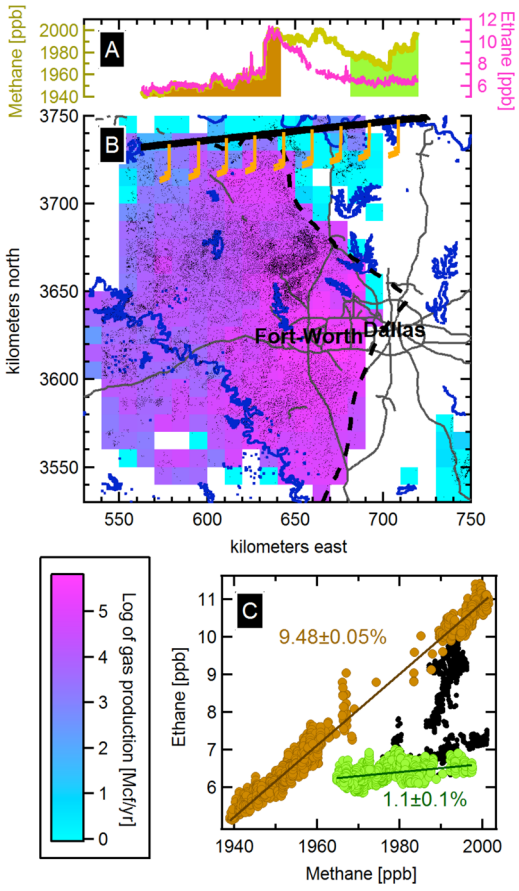

Figure 4. Flight results downwind of the Barnett shale on March 27, 2013. Methane and ethane mixing ratios acquired during flight are plotted versus horizontal distance in Panel A. The map in Panel B shows the flight path (thick black trace) north of the cities of Dallas and Fort-Worth. Wind was consistently from the south at ∼13 ms^{-1} during this transect, as shown by the orange wind barbs along the flight track. Major roads (gray), bodies of water (blue), and approximate boundaries of the Barnett shale formation (dotted line) are also shown. Well locations dot the map (black), and the color map shows binned inventory values for gas production (see text for details). Ethane is plotted vs methane in Panel C, with westerly (orange) and easterly (green) portions of the transect highlighted in Panels A and C.

wind direction for this day is indicated by the wind barbs overlaid on the flight path.

The shale region is densely dotted by both oil and gas wells in the areas surrounding Dallas/Fort Worth (counties outside of the current scope omitted). Inventory numbers for the total yearly gas production from the wells shown are available[43] (cubic feet of gas per year) and are represented in the color scale plot on the map. The values are shown in 10 km × 10 km bins and the logarithm taken to enhance differences. No data is shown in regions without wells.

The mixing ratios for methane and ethane for this trajectory are shown in Panel A of Figure 4 as a function of east−west distance. Following the plane's trajectory from west to east, the ethane and methane mixing ratios increase coincidently with the aircraft moving downwind of an increasing well density. At around 650 km east, the ethane plume begins to fall back toward background, while the methane plume stays relatively elevated. As the plane flies past the boundaries of the Barnett shale, ethane returns to low levels while methane does not. The ethane and methane correlation plot (Panel C in Figure 4)

shows the ethane/methane enhancement ratios defined by these mixing ratio variations. Two regions have been highlighted in orange and in green, corresponding to the western-most and eastern-most portions of the transect. These regions have fairly consistent but differing ethane/methane enhancement ratios of 9.48 ± 0.05% and 1.1 ± 0.1%, respectively (uncertainties from the standard deviation of the slope at 95% confidence). The central region (black points in Panel C) shows transitional ratios.

These regional-scale ethane/methane enhancement ratios demonstrate that the methane emissions in the Dallas/Fort Worth region can be crudely broken down into at least two geographically distinct source regions: the Barnett shale oil and gas field to the west (high in ethane, such as wet gas wells) and the region to the east (low in ethane). In reality, methane emissions in and around Dallas/Fort Worth and the Barnett are characterized by an entire distribution of sources with the possibility of great variations in emission rate, ethane/methane enhancement ratios, and geographic location, each of which will affect the downwind regional-scale enhancement ratios identified above. Of particular interest is the variation in enhancement ratios within the shale formation, since inventory data shows increased oil production in the northern portion of the Barnett (gas production shown in Figure 4).[43] The combination of individual source enhancement ratios from a sampled range of Barnett methane emitters (as in the Measurement of Known Sources section above) with regional-scale measurements (as in Figure 4) may lead to a better understanding of the contributions of different source types to total regional emissions.

These results demonstrate the great potential of continuous ethane measurements in experimental studies of methane emissions, both to distinguish between thermogenic and biogenic sources and in gaining a better understanding of the variety within oil and NG sources.

■ ASSOCIATED CONTENT

Supporting Information

Mobile platform integration, analysis and calibration details, descriptions, time series and analysis for entries in Table 1. This material is available free of charge via the Internet at http://pubs.acs.org.

■ AUTHOR INFORMATION

Corresponding Author

*Phone: 978 663-9500 ext. 266. Fax: 978 663-4918. E-mail: herndon@aerodyne.com.

Author Contributions

All authors have given approval to the final version of the manuscript.

Notes

The authors declare no competing financial interest.

■ REFERENCES

(1) *Annual energy outlook 2013 with projections to 2040*; DOE/EIA-0383(2013); U.S. Energy Information Administration, U.S. Department of Energy: Washington, DC, 2013. www.eia.gov/forecasts/aeo (accessed April 28, 2014).

(2) Allen, D. T.; Torres, V. M.; Thomas, J.; Sullivan, D. W.; Harrison, M.; Hendler, A.; Herndon, S. C.; Kolb, C. E.; Fraser, M. P.; Hill, A. D.; Lamb, B. K.; Miskimins, J.; Sawyer, R. F.; Seinfeld, J. H. Measurements of methane emissions at natural gas production sites in the United States. *Proc. Natl. Acad. Sci. U. S. A.* **2013**, *110*, 17768 DOI: 10.1073/pnas.1304880110.

(3) Karion, A.; Sweeney, C.; Pétron, G.; Frost, G.; Michael Hardesty, R.; Kofler, J.; Miller, B. R.; Newberger, T.; Wolter, S.; Banta, R.; Brewer, A.; Dlugokencky, E.; Lang, P.; Montzka, S. A.; Schnell, R.; Tans, P.; Trainer, M.; Zamora, R.; Conley, S. Methane emissions estimate from airborne measurements over a western United States natural gas field. *Geophys. Res. Lett.* **2013**, *40*, 4393 DOI: 10.1002/grl.50811.

(4) Gathering facts to find climate solutions, 2014. Environmental Defense Fund Website. http://www.edf.org/climate/methane-studies (accessed 01/31/2014).

(5) Katzenstein, A. S.; Doezema, L. A.; Simpson, I. J.; Blake, D. R.; Rowland, F. S. Extensive regional atmospheric hydrocarbon pollution in the southwestern United States. *Proc. Natl. Acad. Sci.* **2003**, *100*, 11975 DOI: 10.1073/pnas.1635258100.

(6) Kort, E. A.; Eluszkiewicz, J.; Stephens, B. B.; Miller, J. B.; Gerbig, C.; Nehrkorn, T.; Daube, B. C.; Kaplan, J. O.; Houweling, S.; Wofsy, S. C. Emissions of CH_4 and N_2O over the United States and Canada based on a receptor-oriented modeling framework and COBRA-NA atmospheric observations. *Geophys. Res. Lett.* **2008**, *35*, L18808 DOI: 10.1029/2008GL034031.

(7) Brandt, A. R.; Heath, G. A.; Kort, E. A.; O'Sullivan, F.; Pétron, G.; Jordaan, S. M.; Tans, P.; Wilcox, J.; Gopstein, A. M.; Arent, D.; Wofsy, S.; Brown, N. J.; Bradley, R.; Stucky, G. D.; Eardley, D.; Harriss, R. Methane leaks from North American natural gas systems. *Science* **2014**, *343*, 733 DOI: 10.1126/science.1247045.

(8) Miller, S. M.; Wofsy, S. C.; Michalak, A. M.; Kort, E. A.; Andrews, A. E.; Biraud, S. C.; Dlugokencky, E. J.; Eluszkiewicz, J.; Fischer, M. L.; Janssens-Maenhout, G.; Miller, B. R.; Miller, J. B.; Montzka, S. A.; Nehrkorn, T.; Sweeney, C. Anthropogenic emissions of methane in the United States. *Proc. Natl. Acad. Sci.* **2013**, *110*, 20018 DOI: 10.1073/pnas.1314392110.

(9) *EIA's proposed definitions for natural gas liquids*; U.S. Energy Information Administration: Washington, DC, 2013. http://www.eia.gov/petroleum/workshop/ngl/ (accessed April 30, 2014).

(10) Whiticar, M. Correlation of natural gases with their sources. In *The petroleum system - from source to trap*; Magoon, L. B., Dow, W. G., Eds.; AAPG: 1994; pp 261−283.

(11) Simpson, I. J.; Sulbaek Andersen, M. P.; Meinardi, S.; Bruhwiler, L.; Blake, N. J.; Helmig, D.; Rowland, F. S.; Blake, D. R. Long-term decline of global atmospheric ethane concentrations and implications for methane. *Nature* **2012**, *488*, 490 DOI: 10.1038/nature11342.

(12) Etiope, G.; Ciccioli, P. Earth's degassing: A missing ethane and propane source. *Science* **2009**, *323*, 478 DOI: 10.1126/science.1165904.

(13) Peischl, J.; Ryerson, T. B.; Brioude, J.; Aikin, K. C.; Andrews, A. E.; Atlas, E.; Blake, D.; Daube, B. C.; de Gouw, J. A.; Dlugokencky, E.; Frost, G. J.; Gentner, D. R.; Gilman, J. B.; Goldstein, A. H.; Harley, R. A.; Holloway, J. S.; Kofler, J.; Kuster, W. C.; Lang, P. M.; Novelli, P. C.; Santoni, G. W.; Trainer, M.; Wofsy, S. C.; Parrish, D. D. Quantifying sources of methane using light alkanes in the Los Angeles basin, California. *J. Geophys. Res., [Atmos.]* **2013**, *118*, 4974 DOI: 10.1002/jgrd.50413.

(14) Pétron, G.; Frost, G. J.; Trainer, M. K.; Miller, B. R.; Dlugokencky, E. J.; Tans, P. Reply to comment on "hydrocarbon emissions characterization in the Colorado Front Range: A pilot study" by Michael A. Levi. *J. Geophys. Res., [Atmos.]* **2013**, *118*, 236 DOI: 10.1029/2012JD018487.

(15) Pétron, G.; Frost, G.; Miller, B. R.; Hirsch, A. I.; Montzka, S. A.; Karion, A.; Trainer, M.; Sweeney, C.; Andrews, A. E.; Miller, L.; Kofler, J.; Bar-Ilan, A.; Dlugokencky, E. J.; Patrick, L.; Moore, C. T.; Ryerson, T. B.; Siso, C.; Kolodzey, W.; Lang, P. M.; Conway, T.; Novelli, P.; Masarie, K.; Hall, B.; Guenther, D.; Kitzis, D.; Miller, J.; Welsh, D.; Wolfe, D.; Neff, W.; Tans, P. Hydrocarbon emissions characterization in the Colorado Front Range: A pilot study. *J. Geophys. Res., [Atmos.]* **2012**, *117*, D04304 DOI: 10.1029/2011JD016360.

(16) Zahniser, M. S.; Nelson, D. D.; McManus, J. B.; Kebabian, P. L. Measurement of trace gas fluxes using tunable diode laser spectroscopy. *Philos. Trans. R. Soc. London, Ser. A* **1995**, *351*, 357.
(17) Güllük, T.; Wagner, H. E.; Slemr, F. A high frequency modulated tunable laser absorption spectrometer for measurements of CO_2, CH_4, N_2O, and CO in air samples of a few cm^3. *Rev. Sci. Instrum.* **1997**, *68*, 230.
(18) Fried, A.; Henry, B.; Wert, B.; Sewell, S.; Drummond, J. R. Laboratory, ground-based, and airborne tunable diode laser systems: Performance characteristics and applications in atmospheric studies. *Appl. Phys. B: Laser Opt.* **1998**, *67*, 317.
(19) Kolb, C. E.; Herndon, S. C.; McManus, B.; Shorter, J. H.; Zahniser, M. S.; Nelson, D. D.; Jayne, J. T.; Canagaratna, M. R.; Worsnop, D. R. Mobile laboratory with rapid response instruments for real-time measurements of urban and regional trace gas and particulate distributions and emission source characteristics. *Environ. Sci. Technol.* **2004**, *38*, 5694.
(20) Herndon, S. C.; Jayne, J. T.; Zahniser, M. S.; Worsnop, D. R.; Knighton, B.; Alwine, E.; Lamb, B. K.; Zavala, M.; Nelson, D. D.; McManus, J. B.; Shorter, J. H.; Canagaratna, M. R.; Onasch, T. B.; Kolb, C. E. Characterization of urban pollutant emission fluxes and ambient concentration distributions using a mobile laboratory with rapid response instrumentation. *Faraday Discuss.* **2005**, *130*, 327 DOI: 10.1039/b500411j.
(21) Nelson, D. D.; McManus, B.; Urbanski, S.; Herndon, S.; Zahniser, M. S. High precision measurements of atmospheric nitrous oxide and methane using thermoelectrically cooled mid-infrared quantum cascade lasers and detectors. *Spectrochim. Acta, Part A* **2004**, *60*, 3325.
(22) Hirst, B.; Gibson, G.; Gillespie, S.; Archibald, I.; Podlaha, O.; Skeldon, K. D.; Courtial, J.; Monk, S.; Padgett, M. Oil and gas prospecting by ultra-sensitive optical gas detection with inverse gas dispersion modelling. *Geophys. Res. Lett.* **2004**, *31*, L12115 DOI: 10.1029/2004GL019678.
(23) Krzempek, K.; Jahjah, M.; Lewicki, R.; Stefański, P.; So, S.; Thomazy, D.; Tittel, F. K. CW DFB RT diode laser-based sensor for trace-gas detection of ethane using a novel compact multipass gas absorption cell. *Appl. Phys. B: Laser Opt.* **2013**, *112*, 461 DOI: 10.1007/s00340-013-5544-9.
(24) Nähle, L.; Belahsene, S.; von Edlinger, M.; Fischer, M.; Boissier, G.; Grech, P.; Narcy, G.; Vicet, A.; Rouillard, Y.; Koeth, J.; Worschech, L. Continuous-wave operation of type-I quantum well DFB laser diodes emitting in 3.4 μm wavelength range around room temperature. *Electron. Lett.* **2011**, *47*, 46 DOI: 10.1049/el.2010.2733.
(25) McManus, J. B.; Kebabian, P. L.; Zahniser, M. S. Astigmatic mirror multiple pass absorption cells for long pathlength spectroscopy. *Appl. Opt.* **1995**, *34*, 3336.
(26) Humlicek, J. Optimized computation of the Voigt and complex probability function. *J. Quant. Spectrosc. Radiat. Transfer* **1982**, *27*, 437.
(27) Harrison, J. J.; Allen, N. D. C.; Bernath, P. F. Infrared absorption cross sections for ethane (C_2H_6) in the 3 μm region. *J. Quant. Spectrosc. Radiat. Transfer* **2010**, *111*, 357 DOI: 10.1016/j.jqsrt.2009.09.010.
(28) Rothman, L. S.; Gordon, I. E.; Babikov, Y.; Barbe, A.; Chris Benner, D.; Bernath, P. F.; Birk, M.; Bizzocchi, L.; Boudon, V.; Brown, L. R.; Campargue, A.; Chance, K.; Cohen, E. A.; Coudert, L. H.; Devi, V. M.; Drouin, B. J.; Fayt, A.; Flaud, J. M.; Gamache, R. R.; Harrison, J. J.; Hartmann, J. M.; Hill, C.; Hodges, J. T.; Jacquemart, D.; Jolly, A.; Lamouroux, J.; Le Roy, R. J.; Li, G.; Long, D. A.; Lyulin, O. M.; Mackie, C. J.; Massie, S. T.; Mikhailenko, S.; Müller, H. S. P.; Naumenko, O. V.; Nikitin, A. V.; Orphal, J.; Perevalov, V.; Perrin, A.; Polovtseva, E. R.; Richard, C.; Smith, M. A. H.; Starikova, E.; Sung, K.; Tashkun, S.; Tennyson, J.; Toon, G. C.; Tyuterev, V. G.; Wagner, G. The HITRAN2012 molecular spectroscopic database. *J. Quant. Spectrosc. Radiat. Transfer* **2013**, *130*, 4 DOI: 10.1016/j.jqsrt.2013.07.002.
(29) Jiménez, R.; Herndon, S.; Shorter, J. H.; Nelson, D. D.; McManus, J. B.; Zahniser, M. S. Atmospheric trace gas measurements using a dual quantum-cascade laser mid-infrared absorption spectrometer. *Proc. Soc. Photo-Opt. Instrum. Eng.* **2005**, *5738*, 318 DOI: 10.1117/12.597130.
(30) Santoni, G. W.; Lee, B. H.; Goodrich, J. P.; Varner, R. K.; Crill, P. M.; McManus, J. B.; Nelson, D. D.; Zahniser, M. S.; Wofsy, S. C. Mass fluxes and isofluxes of methane (CH_4) at a New Hampshire fen measured by a continuous wave quantum cascade laser spectrometer. *J. Geophys. Res.* **2012**, *117*, D10301 DOI: 10.1029/2011jd016960.
(31) Crosson, E. R. A cavity ring-down analyzer for measuring atmospheric levels of methane, carbon dioxide, and water vapor. *Appl. Phys. B: Laser Opt.* **2008**, *92*, 403 DOI: 10.1007/s00340-008-3135-y.
(32) Werle, P.; Mücke, R.; Slemr, F. The limits of signal averaging in atmospheric trace-gas monitoring by tunable diode-laser absorption spectroscopy (TDLAS). *Appl. Phys. B: Laser Opt.* **1993**, 131.
(33) Swanson, A. L.; Blake, N. J.; Atlas, E.; Flocke, F.; Blake, D. R.; Rowland, F. S. Seasonal variations of C_2–C_4 nonmethane hydrocarbons and C_1–C_4 alkyl nitrates at the summit research station in Greenland. *J. Geophys. Res., [Atmos.]* **2003**, *108*, 4065 DOI: 10.1029/2001JD001445.
(34) Marrero, J. University of California, Irvine, CA. Personal communication, 2014.
(35) Keeling, C. D. The concentration and isotopic abundances of carbon dioxide in the atmosphere. *Tellus* **1960**, *12*, 200 DOI: 10.1111/j.2153-3490.1960.tb01300.x.
(36) Coyle, D.; de la Vega, F. F.; Durr, C. *Natural gas specification challenges in the LNG industry*; Paper PS4-7; KBR: Houston, TX, 2007. http://www.kbr.com/Newsroom/Publications/technical-papers/Natural-Gas-Specification-Challenges-in-the-LNG-Industry.pdf (accessed 02/14/2014).
(37) AES ocean express LLC v. Florida gas transmission company and Southern Natural Gas Company. *121 FERC 61.267*, Docket No. RP04-249-006, 2007; Federal Energy Regulatory Commission, Opinion No. 495-A Order on Rehearing.
(38) FERC NGA gas tariff, sixth revised volume no. 1 in; Tennessee Gas Pipeline Company L.L.C.: Houston, TX, 2011; pp 155–156. http://tebb.elpaso.com/ebbmasterpage/Tariff/OrgChart.aspx?code=TGP&status=GQ&pdftag=gtcq (accessed 2/20/2014).
(39) *Heat content of natural gas consumed*; U.S. Energy Information Administration: Washington, DC, 2012. http://www.eia.gov/dnav/ng/ng_cons_heat_a_EPG0_VGTH_btucf_a.htm (accessed April 30, 2014).
(40) Tullo, A. H. Petrochemicals: The U.S. Will see a boom as Europe and Asia struggle. *Chem. Eng. News*, 01/14/**2013**. https://cen.acs.org/articles/91/i2/Petrochemicals-US-see-boom-Europe.html (accessed April 30, 2014).
(41) Hendler, A.; Nunn, J.; Lundeen, J. *VOC emissions from oil and condensate storage tanks*; Houston Advanced Research Center: Houston, TX, 2009. http://files.harc.edu/Projects/AirQuality/Projects/H051C/H051CFinalReport.pdf (accessed April 30, 2014).
(42) Oremland, R. S. Microbial formation of ethane in anoxic estuarine sediments. *Appl. Environ. Microbiol.* **1981**, *42*, 122.
(43) *DI desktop*; Drillinginfo - an International Oil & Gas Intelligence Company: Austin, TX, 2013.